Solid Earth

Open Access

A new model of the upper mantle structure beneath the western rim of the East European Craton

M. Dec[1], M. Malinowski[1], and E. Perchuc[2]

[1]Institute of Geophysics, Polish Academy of Sciences, Ks. Janusza 64, 01-452 Warsaw, Poland
[2]Bernardynska 21/57, 02-904 Warsaw, Poland

Correspondence to: M. Dec (monikadec@igf.edu.pl) and E. Perchuc (perchuc.ed.geo@gmail.com)

Abstract. We present a new 1-D P wave seismic velocity model (called MP1-SUW) of the upper mantle structure beneath the western rim of the East European Craton (EEC) based on the analysis of the earthquakes recorded at the Suwałki (SUW) seismic station located in NE Poland which belongs to the Polish Seismological Network (PLSN). Motivation for this study arises from the observation of a group of reflected waves after expected $P_{410}P$ at epicentral distances 2300–2800 km from the SUW station. Although the existing global models represent the first-arrival traveltimes, they do not represent the full wavefield with all reflected waves because they do not take into account the structural features occurring regionally such as 300 km discontinuity. We perform P wave traveltime analysis using 1-D and 2-D forward ray-tracing modelling for the distances of up to 3000 km. We analysed 249 natural seismic events from four azimuthal spans with epicentres in the western Mediterranean Sea region (WMSR), the Greece and Turkey region (GTR), the Caucasus region (CR) and the part of the northern Mid-Atlantic Ridge near the Jan Mayen Island (JMR). For all chosen regions, except the JMR group for which 2-D modelling was performed, we estimate a 1-D average velocity model which will characterize the main seismic discontinuities. It appears that a single 1-D model (MP1-SUW model) explains well the observed traveltimes for the analysed groups of events. Differences resulting from the different azimuth range of earthquakes are close to the assumed picking uncertainty. The MP1-SUW model documents the bottom of the asthenospheric low-velocity zone (LVZ) at the depth of 220 km, 335 km discontinuity and the zone with the reduction of P wave velocity atop 410 km discontinuity which is depressed to 440 km depth. The nature of the regionally oc-
curring 300 km boundary is explained here by tracing the ancient subduction regime related to the closure of the Iapetus Ocean, the Rheic Ocean and the Tornquist Sea.

1 Introduction

One-dimensional reference models are employed almost in every seismological method aimed at imaging of Earth's interior (tomography, receiver functions, underside reflections). However, results of those methods can be biased by the choice of the background velocity model (e.g. Bastow, 2012). Therefore, in the regional studies, it might be more appropriate to use modified reference models taking into account, e.g. the tectonic regime of the area (e.g. Perchuc and Thybo, 1996). Following this strategy, we attempt to derive a one-dimensional upper mantle P wave velocity model for the areas surrounding the East European Craton (EEC) to the west and to the south. Toward this end, we use the data recorded at the Suwałki (SUW) station belonging to the Polish Seismological Network. The data recorded at the SUW station were used in few seismological studies (e.g. Bock et al., 1997; Świeczak et al., 2004; Wilde-Piórko, 2005), but none of these were focusing on the detailed interpretation of the recorded traveltimes in the far-regional mode.

Due to the advancement in instrumentation and access to infrastructure, array seismology is developing rapidly (e.g. the Earthscope USArray project; Levander, 2003). However, the cost of experiments remain very high. Here we would like to explore the concept of using single-station data from the existing seismological network to study the upper mantle structure based on the traveltimes and amplitudes of the
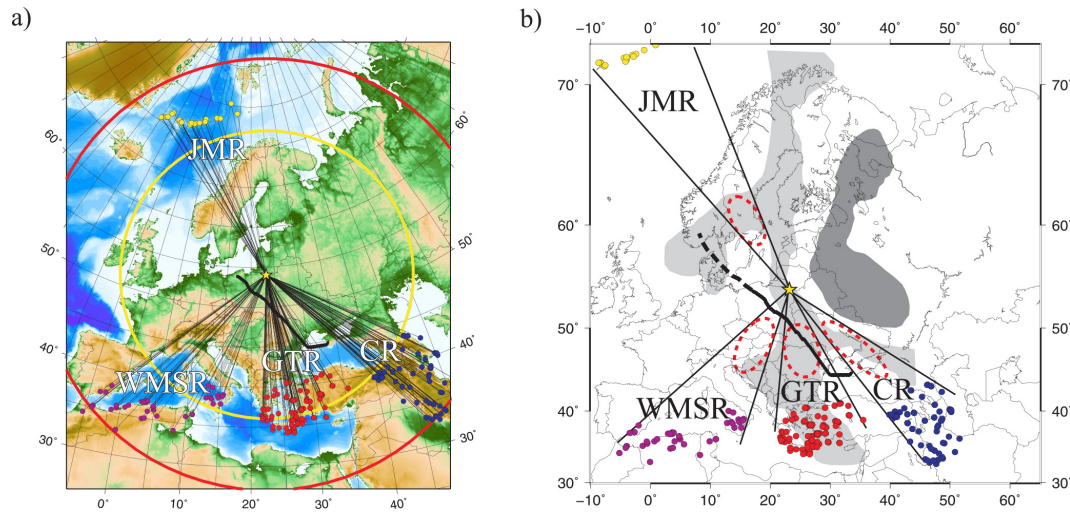
Figure 1. (a) Four groups of earthquakes recorded at the SUW station (yellow asterisk): JMR (yellow points), WMSR (violet points), GTR (red points) and CR (blue points). Circles centred at SUW mark the distance of 2000 (yellow) and 3000 km (red). Thick black line represents the TTZ. **(b)** Map of the study area with indication of the regions to which our upper mantle model pertains (red dashed ellipses). Areas shaded in grey are characterized by higher S wave velocities at 250 km depth according to the model of Shapiro and Ritzwoller (2002). Light grey represents velocities about 4.65 km s^{-1} and dark grey about 4.80 km s^{-1}.

body waves. The necessary prerequisite for performing such a study is the selection of the station that is located optimally for imaging particular mantle structure by providing proper azimuthal span and epicentral distances of the recorded earthquakes (see e.g. Nita et al., 2012).

The choice of the SUW station for this analysis is twofold. First of all, it is characterized by a good signal-to-noise ratio and relatively simple wavefield, as it is located on the stable part of the EEC with a thin sedimentary cover. Secondly, the earthquakes recorded from the four azimuthal sectors (northern Mid-Atlantic Ridge, Western Mediterranean Sea, Greece–Turkey, and Caucasus) are located in the 1500–3000 km epicentral distance range, providing proper illumination of the upper mantle structure between the base of the asthenosphere and the 410 km discontinuity. The bottoming points of the refracted waves and midpoints of the reflected waves fall in to the south-western rim of the East European Craton as indicated in Fig. 1. Therefore, we can study the influence of the Teisseyre–Tornquist zone (TTZ) on the recorded wavefield and mantle structure.

First, we present the tectonic setting and a review of the studies pertaining to the investigated area, which mainly focused on Earth's crust. Subsequently, we describe data (seismic waveforms from natural seismic events) and methods used in this analysis (1-D and 2-D ray-tracing modelling). In the results section we present all analysed seismic sections together with the traveltimes calculated for our preferred upper mantle model. It is followed by error analysis and traveltime residuals statistics. Finally, we discuss our results in the context of the geodynamics of the circum-EEC region.

2 Tectonic setting and previous geophysical investigations

In order to understand the structure and nature of the upper mantle below the Baltica, it is necessary to understand its history as a palaeocontinent which was moving across Iapetus Ocean with other palaeocontinents and microplates which are nowadays neighbouring Baltica. The EEC is the oldest part of eastern Europe. It formed about 1.8–1.7 Ga (years ago) as a result of a collision between three separate plates: Fenoscandia, Sarmatia and Volgo-Uralia (Bogdanova et al., 2001, Bogdanova et al., 2005). The history of the palaeoplate movements from Vendian to Permian was described by Cocks and Torsvik (2006). There were two major palaeotectonical events. First, about 450 Ma in the Ordovician, Avalonia separated from Gondwana and docked with Baltica and afterwards they both joined Laurentia. The last event was connected with the closure of the Iapetus Ocean which ended about 420 Ma and the closure of the Tornquist Sea – a branch of Iapetus. A different situation had place in the SW part of the cratonic rim. In this area there were Rheic Ocean structures formed from Devonian to Permian and then the Palaeotethyan, which were evolving up to the TTZ (Ziegler et al., 2006). Caledonian structures: Northwest Highlands (Gee, 1975) and Polish Caledonides (Znosko, 1986) were imposed on the NW and SW margins of the EEC.

Geophysical studies are mainly seismic. There were numerous deep seismic sounding profiles recorded both west and east of the TTZ (see recent summary in Guterch et al., 2010). Starting with the LT profiles located in Poland (Guterch et al., 1986), through the EUGENO-S project

in Denmark and southern Sweden (EUGENO-S Working Group et al., 1988), Polish projects POLONAISE'97 (Guterch et al., 1999) and CELEBRATION 2000 (Guterch et al., 2001), the FENNOLORA transect (Guggisberg and Berthelsen, 1987; Abramovitz et al., 2002), the BABEL project (BABEL Working Group, 1991), the MONA LISA (Abramovitz et al., 1998) or EUROBRIDGE projects (EUROBRIDGE Seismic Working Group, 1999) we have a good control on the crustal structure of the EEC and surrounding areas.

All of these projects provided gross crustal structure down to the Moho and only in few cases were deeper boundaries interpreted (e.g. Grad et al., 2002). During the acquisition of the deep seismic sounding profiles, some upper mantle phases (both reflections and refractions) were traced in the offset range beyond 400 km (e.g. in project POLONAISE'97, Grad et al., 2002; EUGENO-S Working Group, 1988; BABEL Working Group, 1993; MONA LISA, Abramovitz et al., 1999). Apart from the controlled-source seismology, some passive-source experiments were conducted with the TOR project being the most significant (Gregersen et al., 2010; Plomerova et al., 2002). The TOR project spanning about 1000 km from northern Germany, through Denmark up to southern Sweden, crossed principal tectonic zones inside the rim of the EEC such as the Variscan Front, the Caledonian Deformation Front and the Sorgenfrei–Tornquist zone – the northern extension of the TTZ. This allowed us to image seismic structure of the crust and upper mantle (e.g. Somali et al., 2006, Gregersen et al., 2010). The recently conducted PASSEQ project (Wilde-Piórko et al., 2008) provided new data for studying mantle structure across the TTZ, e.g. using teleseismic P wave receiver functions (Knapmeyer-Endrun et al., 2013).

3   Data and method

The SUW seismic station was chosen for this study because of the good recording conditions in the remote part of NE Poland and the thin sediment cover resulting in high-quality seismic signal registrations. The station is equipped with the STS-2 sensor and the data are recorded at 20 Hz. We used broadband data recorded between 1997 and 2010 for earthquakes with magnitude greater than 4.5. The hypocentre locations were taken from the ISC bulletin (International Seismological Centre; http://www.isc.ac.uk/iscbulletin). The retrieved waveforms were converted from the native MSEED to SEG-Y format in order to make seismic record sections suitable for interpretation and modelling using standard tools used in controlled-source seismology (Zelt, 1994).

The 249 events analysed (see Supplement and Fig. 1) are located in the following areas:

Table 1. Mean signal-to-noise ratio for the analysed groups of events.

Region	Number of events	Signal-to-noise ratio		
		Raw data	After filtering (0.5–2.0 Hz)	Improvement (%)
JMR	34	4.70	8.17	73.83
CR 020	34	2.57	7.50	191.83
CR 2050	23	3.52	6.66	89.20
CR 50+	12	5.54	12.66	128.52
GTR 020	53	6.59	4.85	−26.40
GTR 2050	36	3.61	5.26	45.71
GTR 50+	14	13.84	18.02	30.20
WMSR	43	6.30	11.54	83.17
Average		5.38	8.16	67.76

1. rift zone around the Jan Mayen region in the northern Atlantic (JMR)

2. Western Mediterranean Sea region (WMSR)

3. Greece and Turkey region (GTR)

4. Caucasus region (CR).

All earthquakes generated in the JMR (part of the Mid-Atlantic Ridge) (Fig. 2a) were shallow crustal ones (depth down to 10 km). The earthquakes in the WMSR were also shallow, with focal depths down to 20 km (Fig. 2b). However, the data from the GTR (Fig. 2c) and CR (Fig. 2d), due to a large variability of the source depths, were separated into three groups with the focal depth ranges: 0–20 km, 20–50 km and > 50 km. We divided earthquakes into these focal depth ranges after evaluating differences in traveltimes calculated for different focal depths in the AK135 model (Kennett et al., 1995). Modelling was performed for each group separately. It allowed us to limit static shifts in the record sections to 1 s. We did not apply focal depth corrections to the data belonging to each epicentral group.

Seismic record sections sorted according to the increasing epicentral distance consist of the following number of seismograms: 34 (JMR), 43 (WMR), 103 (GTR), 69 (CR). We tested a range of bandpass filter frequencies for displaying data and finally we concluded that the best results were obtained for a 0.5–2.0 Hz bandwidth. This bandpass filter is commonly used in analysing data recorded in the far-regional mode (e.g. Chu et al., 2012; Świeczak et al., 2004). As a data quality check we calculated the signal-to-noise (SNR) ratio, estimated using energy of the signal in the 2 s wide window before and after first arrivals. Calculations were made using the ZPLOT software (Zelt, 1994). Table 1 shows mean SNRs calculated for the individual group of events. Group of the deepest earthquakes from the GTR are characterized by the best SNR for raw data. The best improvement after filtering was observed for the CR group for events with focal depths between 0 and 20 km. The average SNR for all raw data is
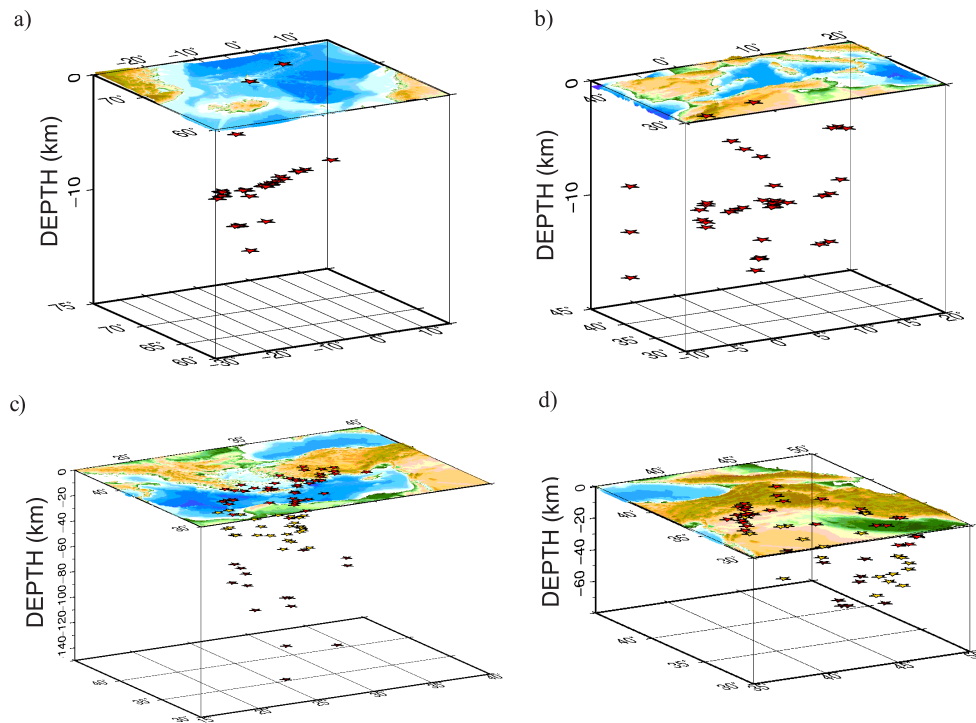
Figure 2. Distribution of the focal depths for the analysed groups of earthquakes: **(a)** JMR, **(b)** WMSR, **(c)** GTR, **(d)** CR.

Table 2. List of seismic events shown in Fig. 3. Numbers from column 1 correspond to numbers of seismic records in Fig. 3. (UTC – coordinated universal time)

No.	Offset (km)	Date	Origin time (UTC)	Lat	Long	Depth (km)	Mag (mb)	Seismic region
1	2259.18	24 Jun 2002	01:20:37.60	35.92	9.88	10.0	4.7	Tunisia
2	2267.73	25 Feb 2007	21:53:13.80	73.18	6.77	10.0	5.1	Greenland Sea
3	2275.16	07 Jun 1999	16:10:33.66	73.02	5.35	10.0	5.2	Greenland Sea
4	2307.27	30 Aug 2005	20:53:48.17	71.91	−1.09	10.0	4.8	Jan Mayen Island region
5	2322.30	08 Sep 2008	21:17:15.10	72.63	0.96	10.0	5.0	Norwegian Sea
6	2323.20	26 Aug 1999	05:03:05.04	71.70	−2.43	10.0	5.1	Jan Mayen Island region
7	2334.51	02 Dec 1997	00:02:03.51	71.65	−3.03	10.0	5.0	Jan Mayen Island region
8	2340.29	13 Aug 2006	19:03:08.50	71.39	−4.00	13.1	4.8	Jan Mayen Island region
9	2360.94	23 Mar 1998	20:19:27.74	71.50	−4.47	10.0	5.1	Jan Mayen Island region
10	2392.71	22 May 2003	13:57:21.27	37.12	3.84	10.0	4.8	Western Mediterranean Sea
11	2395.07	16 Nov 2000	11:33:08.87	36.63	4.79	8.7	4.8	Northern Algeria
12	2402.14	22 May 2003	03:14:04.85	37.16	3.57	15.0	5.2	Western Mediterranean Sea
13	2412.09	02 Sep 2008	20:00:50.82	38.72	45.79	3.0	4.9	Iran–Armenia–Azerbaijan border
14	2421.17	19 Jun 2003	12:59:23.14	71.08	−7.64	0.5	5.6	Jan Mayen Island region
15	2422.18	14 Apr 2004	23:07:37.81	71.05	−7.74	10.5	5.7	Jan Mayen Island region
16	2424.21	27 May 2003	17:11:28.35	36.94	3.54	6.1	5.5	Northern Algeria
17	2430.11	18 Aug 2000	18:15:06.54	36.19	4.96	10.0	4.9	Northern Algeria

5.38 and after bandpass filtering we achieve improvement of ∼ 68 %. Therefore, all presented seismic sections are displayed with a 0.5–2.0 Hz bandpass filter.

In this work we analysed earthquakes recorded in the far-regional mode, i.e. with epicentral distances of 1500–3000 km. As shown, for example, by Thybo and Perchuc (1997), this offset range allows one to study upper mantle structure between the Lehman discontinuity at ca. 200 km depth and the 410 km discontinuity. Phase identification was supported by aligning the observed reflectivity based on the maximum amplitude (Fig. 3) for earthquakes from different azimuthal spans (Table 2). Good alignment was obtained for the phase emerging at the time characteristic of the 410 km discontinuity (Fig. 3a). There are also some other
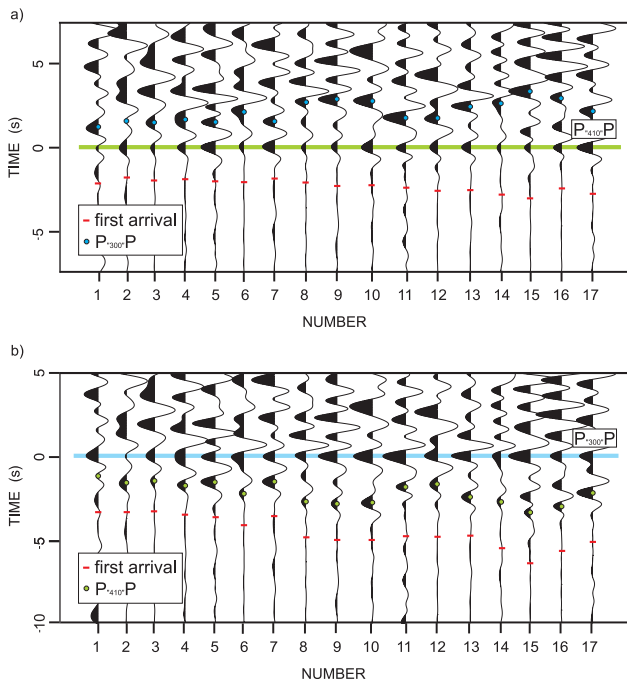
Figure 3. Seismograms aligned by the maximum amplitudes of **(a)** $P_{410}P$ (green line) and **(b)** $P_{300}P$ (blue line). Seismograms are ordered by the event's number (see Table 2). Red dashes represent first arrivals. Blue dots in **(a)** correspond to blue line in **(b)**. Green dots in **(b)** correspond to green line in **(a)**.

strong phases that can be aligned in the epicentral distance of 2260–2430 km (Fig. 3b), later interpreted as being the reflection phases from around 300 km depth. The discontinuity at ca. 300 km was introduced based on earlier results of Nita et al. (2012) and the presence of the reflected arrivals above the $P_{410}P$ reflected phase. The following reflected and refracted seismic phases were interpreted in the record sections (Figs. 4–7) during subsequent modelling: P_{220} – refracted wave from the bottom of the asthenosphere (LVZ), $P_{335}P$ – reflected wave from the regionally occurring discontinuity located at the depth of about 335 km, and P_{440} and $P_{440}P$ – refracted and reflected waves from depressed 410 km discontinuity, modelled at ca. 440 km depth.

We used forward trial-and-error one-dimensional (Kamiński and Muller, 1979) or two-dimensional ray-tracing modelling (Gorman, 2002) in order to fit the observed traveltimes of the refracted and reflected P wave mantle phases and derive upper mantle P wave velocity models beneath the areas indicated in Fig. 1b. We use spherical earth conversion in 1-D modelling and spherical earth 2-D ray-tracing in case of 2-D modelling. We picked first arrivals (P_{220} and P_{440}) and reflected waves from discontinuities at the depths of 220, 335 and 440 km ($P_{220}P$, $P_{335}P$ and $P_{440}P$ respectively). Finally, models were verified by calculating synthetic seismograms using the reflectivity method (Fuchs and Muller, 1971; Muller, 1985).

4   Results

We begin our modelling with the analysis of the MP-1 model derived for the seismically active part of the United States (Perchuc et al., 2008), west of the North American Craton. The North American Craton was created in the same time as the EEC (Hoffman, 1988) and is characterized by similar features, which justifies such an analysis. For all chosen regions in this analysis we try to estimate a 1-D average model which will characterize the main seismic discontinuities. It came out during the modelling that a single 1-D model (MP1-SUW model) explains well the observed traveltimes for the four groups of events analysed. Differences resulting from the different azimuth range of earthquakes are close to the assumed picking uncertainty (0.1 s).

Figure 4a shows the obtained velocity distribution beneath the western rim of the EEC (MP1-SUW model, Table 3) resulting from the forward ray-tracing modelling and fitting of the calculated traveltimes to the observed mantle arrivals (Figs. 4–7). Because of the far-regional offset range used in this study, the velocities in the crust and down to 8° discontinuity (ca. 100 km depth; Thybo and Perchuc, 1997) and within the asthenosphere were introduced a priori and fixed during modelling. The crustal part of the models was based on the published deep seismic sounding results (e.g. Guterch et al., 1996; Grad et al., 2009). In case of the JMR group, the waves leaving the source propagated within the oceanic crust first and then went through the continental-type lithosphere. Therefore, 2-D modelling was necessary to account for the variability between the oceanic and continental lithosphere encountered along this transect (Fig. 7b). The continental part has a similar vertical distribution of velocity to 1-D models for other azimuths.

Figure 4 shows the seismic sections for the GTR area. Most of the events in this region occur down to 20 km depth and the epicentral distances for those events are from 1500 to 2300 km (Fig. 4b). There is a good fit between the data and the traveltimes refracted at the base of the mantle LVZ (red dashed line) at the depth of 220 km. It is observed in the first arrivals up to 2100 km. The $P_{335}P$ (blue line) occurs as secondary arrivals. At an epicentral distance of about 2100 km, there is an intersection of the traveltime branches of P_{220} and P_{440} (green dashed line) phases. After 2100 km, the offset branch of P_{440} (green dashed line) is observed in first arrivals.

Figure 4c shows the earthquakes from the focal depth range of 20–50 km. These events were recorded at epicentral distances ranging from 1500 to 2300 km. As in the previous group, the P_{220} phase is observed in first arrivals at distances up to about 2100 km. After 2100 km the P_{440} phase arrives first. The $P_{335}P$ wave is also visible as a second group. $P_{440}P$ is also recorded in the form of high-amplitude signals observed at distances from 1950 to 2300 km. The closer the distance of 2250 km, the more difficult it is to separate $P_{335}P$
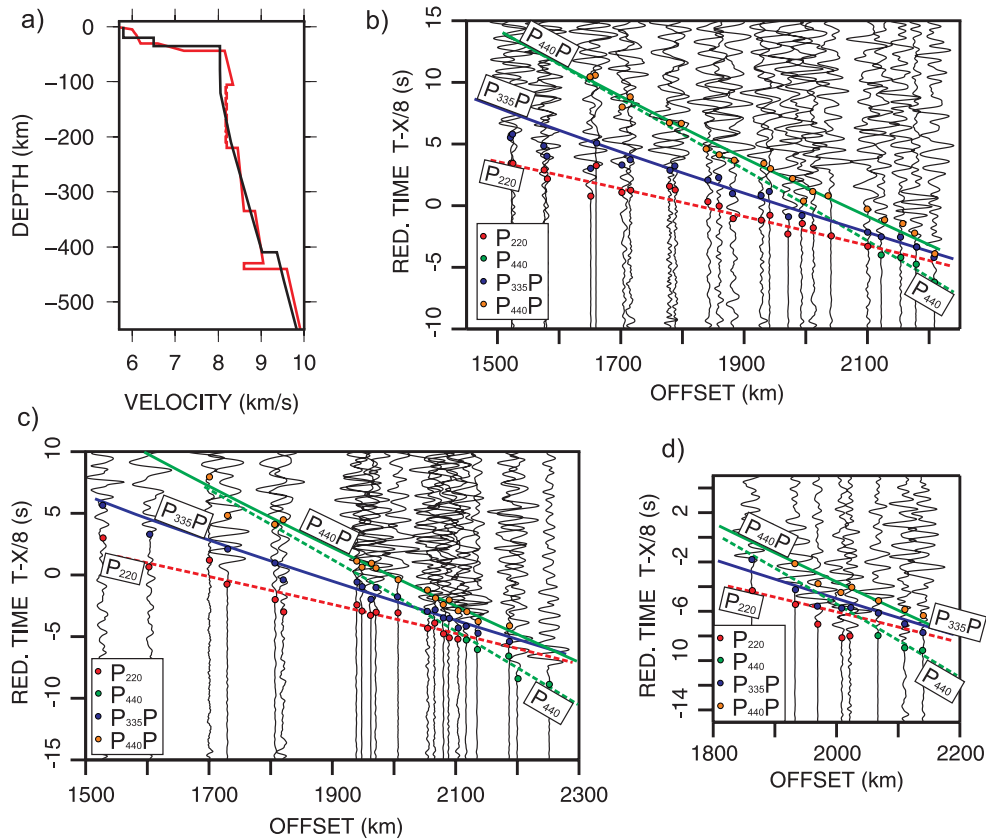
Figure 4. (a) The new MP1-SUW model (red line) compared with the AK 135 model (black line). **(b–d)** Seismic sections with traveltimes calculated for the MP1-SUW model for three focal depth ranges **(b)** 0–20 km, **(c)** 20–50 km, and **(d)** > 50 km. Red dots represent P_{200}, green – P_{440}, blue – $P_{335}P$, and orange – $P_{440}P$ phases.

and $P_{440}P$ because these two branches intersect each other at this point.

Figure 4d shows the deepest group of earthquakes (focal depth > 50 km) recorded at the epicentral distances of 1860 to 2140 km. P_{220} can be seen only on two seismograms. Although, its presence at this depth is documented in the previous two sections. On this section the $P_{335}P$ and $P_{440}P$ reflected phases are also observed.

Figure 5 shows the seismic sections for the CR. Records from these events start at about 2000 and end at about 3000 km epicentral distance. Here we also divided data into three focal depth ranges: 0–20 km depth (Fig. 5a), 20–50 km depth (Fig. 5b) and > 50 km (Fig. 5c). In this case, we can only observe first arrivals of P_{220} in the first two sections (red dashed line). However, analysis of the wavefield allows us to follow phases refracted from 440 km and reflected from 335 and 440 km. On each section we have records documenting intersection of the two branches: $P_{335}P$ and $P_{440}P$ at 2250 km, after which we observed $P_{440}P$ and then $P_{335}P$ as secondary arrivals.

In the case of the WMSR group of events, there is almost the whole range of the useful epicentral distances. The shallow focal depth range, 0–20 km, allows us to put all events

together in one seismic section (Fig. 6). Here we can observe P_{220} as first arrivals at distances from 1700 to 2000 km. At these distances we observe high-amplitude $P_{335}P$ and $P_{440}P$ as secondary arrivals. There is a lack of seismograms in the area where traveltime branches of P_{220} and P_{440} intersect, but after 2200 km we observe P_{440} as first arrivals. Next we interpreted $P_{440}P$ phase followed by the $P_{335}P$ phase.

Figure 7a presents the seismic section for the JMR region. All those earthquakes are located along the rift zone close to the Jan Mayen Island in the northern Atlantic. Their focal depths are from 0 to 10 km. The recorded epicentral distances ranging from 2260 to 2720 km allow us to model 335 and 440 km discontinuities. Taking into account differences in the oceanic and continental lithosphere, we build a 2-D velocity model. We observe P_{440} as first arrivals and $P_{440}P$ as secondary arrivals. The $P_{335}P$ can be also distinguished in this seismic section. Figure 7b illustrates ray-paths for reflection at 335 km depth and refraction and reflection at 440 km discontinuity.

Figure 8 presents all 249 earthquakes with focal-depth traveltime corrections applied in one seismic section. We added values consequent from different focal depths for each group respectively. These values were calculated during the
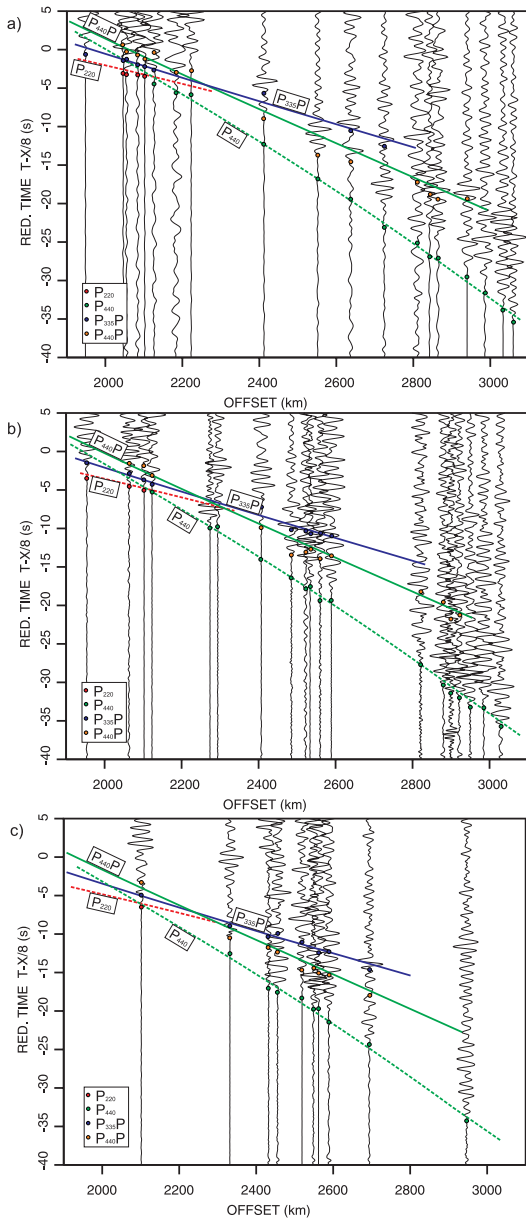
Figure 5. Seismic sections based on the data from the CR group with traveltimes calculated for the MP1-SUW model for three focal depth ranges **(a)** 0–20 km depth, **(b)** 20–50 km depth, and **(c)** >50 km. Red dots represent P_{200}, green – P_{440}, blue – $P_{335}P$, and orange – $P_{440}P$ phases.

Figure 6. Seismic section based on data from the WMSR region with traveltimes calculated for the MP1-SUW model. Red dots represent P_{200}, green – P_{440}, blue – $P_{335}P$, and orange – $P_{440}P$ phases.

Figure 7. (a) Seismic section for the data from the JMR region with traveltimes calculated in the 2-D model shown in **(b)**. **(b)** 2-D ray-tracing model and the ray paths refracted and reflected at 335 and 440 km discontinuities. Green dots represent P_{440}, orange – $P_{440}P$ phases, and blue – $P_{335}P$. Green pattern in the LVZ is used to represent heterogeneous nature of this layer modelled as thin low–high-velocity layers.

separation of earthquakes into smaller groups. In order to verify the credibility of the derived models, we calculated synthetic seismograms using the reflectivity method (Fuchs and Muller, 1971; Muller, 1985). There is a good amplitude match between the recorded data (Fig. 8) and the synthetic section (Fig. 9).

There is an interesting feature in the MP1-SUW model presented here (Fig. 4a). Atop the 440 km discontinuity there is a 10 km thick zone with reduced velocities. The insertion
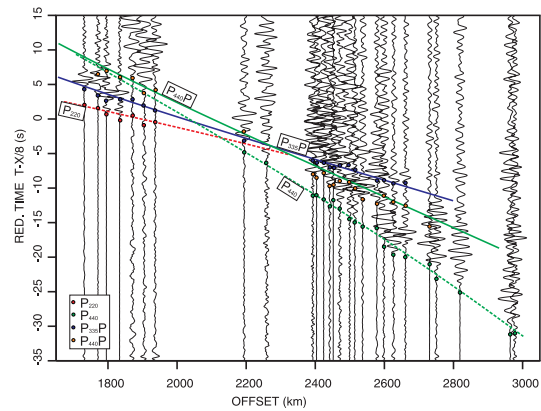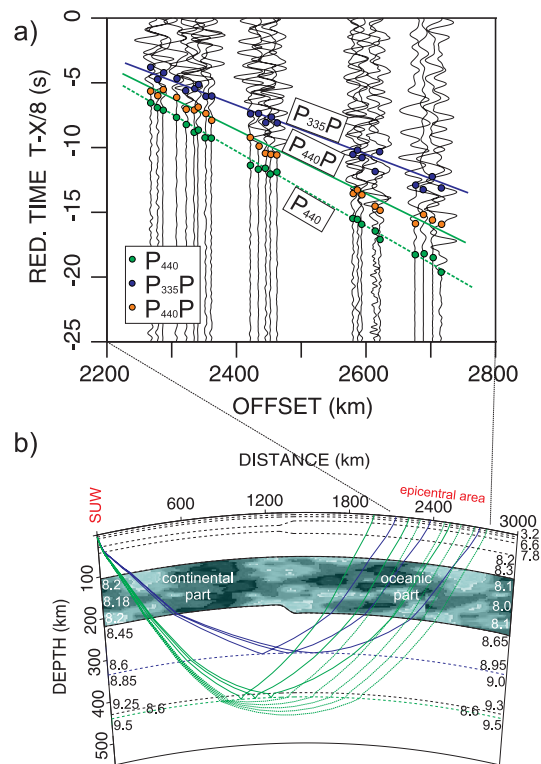
of the LVZ is necessary to explain the separation between P_{440} and $P_{440}P$ branches as shown in Fig. 10. Figure 10a contains part of a section from Fig. 8 with the traveltimes
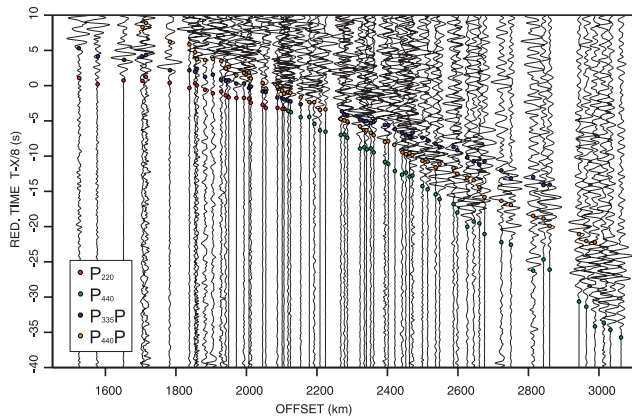
Figure 8. All analysed seismograms recorded at the SUW station with the focal depth corrections applied. Red dots represent P_{200}, green – P_{440}, blue – $P_{335}P$, and orange – $P_{440}P$ phases.
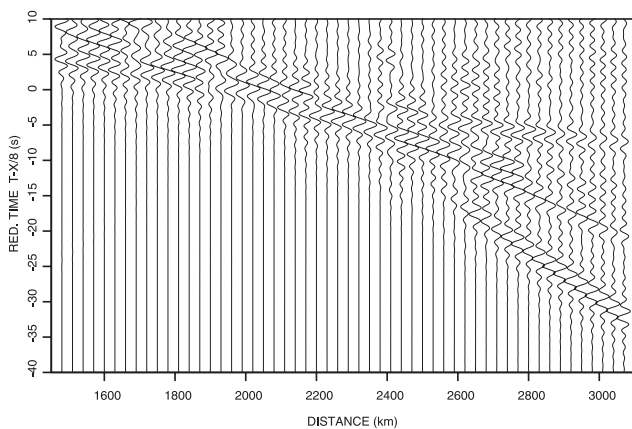

Figure 9. Synthetic seismograms section calculated for the MP1-SUW model using the reflectivity method (0.1–2.0 Hz). Compare with data in Fig. 8.

calculated for the MP1-SUW model and Fig. 10b shows the same section with the traveltimes calculated for the model without the LVZ but with the same average velocity preserved.

5 Error analysis

We picked all the phases with the accuracy of ± 0.1 s. The most significant uncertainties are attributed to the limited accuracy of the event location. The focal depth is the most uncertain hypocentre coordinate in the ISC bulletins, which were used in this analysis.

In order to demonstrate how well the predicted traveltimes fit to the observed data, we present histograms of traveltime residuals ($t_{obs} - t_{calc}$) in Fig. 11. We compare the traveltime residuals of the first arrivals calculated for the MP1-SUW

Table 3. The MP1-SUW P wave velocity model.

Depth (km)	P wave	Depth (km) velocity (km s^{-1})	P wave velocity (km s^{-1})
0	5.60	160	8.20
5	6.00	170	8.20
10	6.05	170	8.18
15	6.10	180	8.18
30	6.20	180	8.20
30	6.60	190	8.18
44	7.20	190	8.20
44	8.15	200	8.20
105	8.35	200	8.18
105	8.20	210	8.18
110	8.20	210	8.20
110	8.18	220	8.20
120	8.18	220	8.45
120	8.20	335	8.60
130	8.20	335	8.85
130	8.18	430	9.05
140	8.18	430	8.60
140	8.20	440	8.60
150	8.20	440	9.60
150	8.18	620	10.10
160	8.18		

model (Fig. 11a–e) and for the reference AK135 model (Kennett et al., 1995) (Fig. 11a'–e').

Figure 11a and 11a' show histograms for all earthquakes used. The adjustment for our model is better than for the AK135. There are smaller errors for the -0.5–0.5 s range. The best fit was obtained for the Jan Mayen group of events (Fig. 11d). The traveltime residual range for that region is ± 1 s. We attribute such a good fit to small focal depth uncertainties of the earthquakes from that region. Events with small focal differences are more unique. It could also be a result of the two-dimensional modelling.

The MP1-SUW model predicts two new branches of traveltimes for reflected waves, the $P_{335}P$ and $P_{440}P$. Figure 12 presents how they fit in the records collected at the SUW station. In the case of other models, such as PREM (Preliminary Reference Earth Model; Dziewoński and Anderson, 1981), IASPEI91 (International Association of Seismology and Physics of the Earth's Interior; Kennett and Engdahl, 1991), AK135 (Kennett et al., 1995) or iPREF (Cammarano and Romanowicz, 2008) there is no possibility to make such analysis because they do not reflect regional-scale inhomogeneities.

In Table 4 we summarized the three parameters of the fitting quality: the standard deviation, variance, kurtosis and root mean square for all groups of data. Kurtosis is a measure of the deviation from the normal distribution (the kurtosis of the normal distribution is 3 for the applied formula). Distributions that have higher variation than the normal
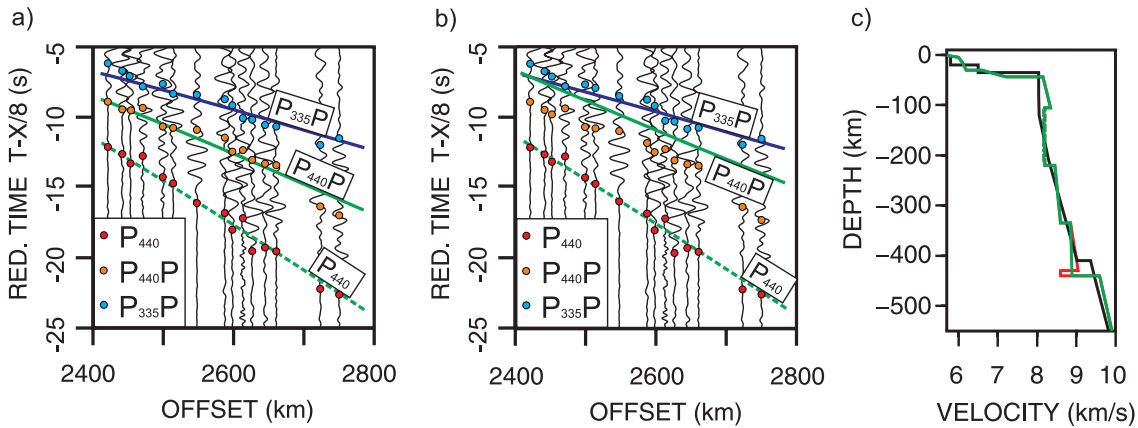
Figure 10. (a) Part of the seismic section with the MP1-SUW model traveltimes overlaid. Red dots represent P_{440}, orange – $P_{440}P$, and blue – $P_{335}P$. **(b)** Part of the seismic section with the traveltimes calculated for the model without the LVZ atop the 440 km discontinuity. **(c)** Comparison of 1-D seismic velocity models. Red line corresponds to the MP1-SUW model and green line to the same model without LVZ atop 440 km discontinuity. Black line corresponds to the AK135 model.

Table 4. Statistics of the traveltime residuals for the MP1-SUW (in bold) and the AK135 models (rms – root-mean square).

Region	Number of events	Standard deviation	Variation	Kurtosis	RMS
Greece and Turkey region	103	1.01	1.01	4.46	1.00
		1.99	3.96	3.62	2.25
Greece and Turkey 0–20	53	**0.85**	**0.73**	**3.32**	**0.88**
		1.80	3.25	3.74	3.03
Greece and Turkey 20–50	36	**1.10**	**1.22**	**6.18**	**1.10**
		1.40	1.96	3.76	1.43
Greece and Turkey 50+	14	**1.18**	**1.40**	**2.69**	**1.20**
		1.29	1.65	2.76	1.44
Caucasus region	69	1.50	2.26	3.45	1.46
		1.61	2.59	2.79	1.65
Caucasus 0–20	34	**1.67**	**2.78**	**2.33**	**1.64**
		1.86	3.44	2.21	1.87
Caucasus 20–50	23	**1.58**	**2.51**	**4.38**	**1.55**
		1.55	2.40	3.52	1.59
Caucasus 50+	12	**0.77**	**0.60**	**3.08**	**0.74**
		0.86	0.73	3.65	1.13
Western Mediterranean Sea region	43	1.20	1.44	3.57	1.19
		1.57	2.46	2.15	1.63
Jan Mayen region	34	0.32	0.10	2.22	0.36
		0.27	0.07	2.63	0.29
All events	249	1.08	1.31	3.72	1.07
		1.58	2.79	3.00	1.71
$P_{335}P$	83	**0.75**	**0.56**	**3.91**	**0.75**
$P_{440}P$	76	**0.75**	**0.57**	**4.00**	**0.80**

distribution have a kurtosis greater than 3, distributions with lower variation have a kurtosis less than 3.

The presented summary of the traveltime residuals' statistics shows the fitting parameters with respect to the MP1-SUW model and the AK135 respectively. We subdivided GTR and CR analysis into smaller groups according to their focal depths. The calculated residuals are also smaller for the JMR. The comparison of the data in Table 4 shows that the experimental data is described better by our model than the global reference AK135 model. Although the AK135 model describes first arrivals well, it does not take into account reflected waves and regional discontinuities such as the 300 km discontinuity.
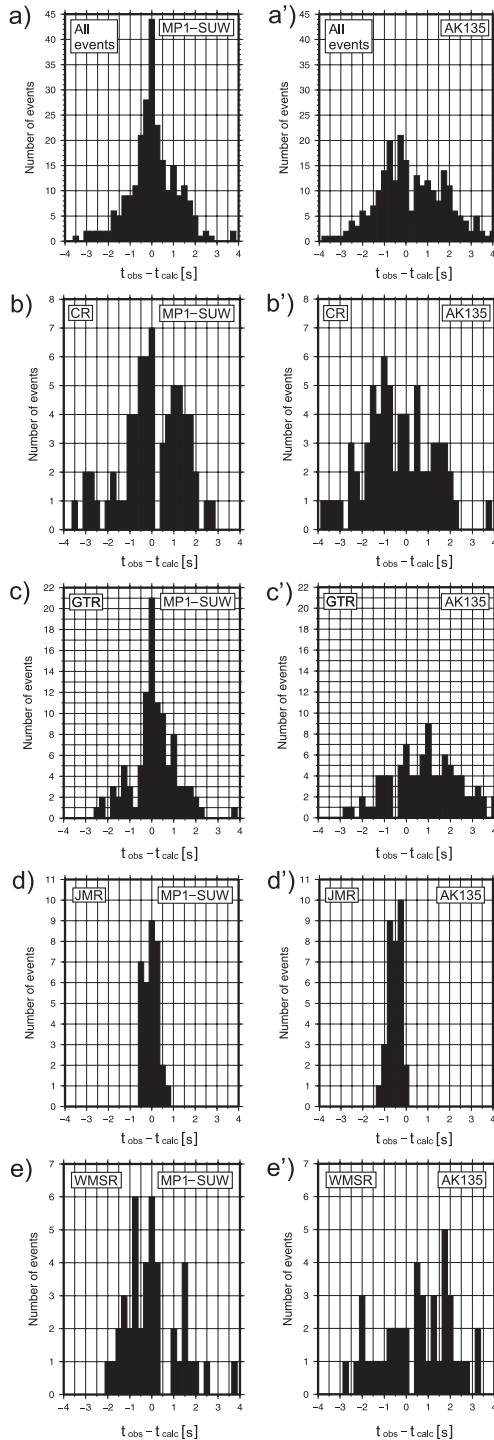
Figure 11. Histograms of the residuals between the observed travel-times and the traveltimes calculated for the MP1-SUW model (left column) and between the observed traveltimes and the traveltimes calculated for the AK135 model (right column) for the following data: **(a)** **(a')** all events, **(b)** **(b')** events from the CR, **(c)** **(c')** events from the GTR , **(d)** **(d')** events from the JMR, **(e)** **(e')** events from the WMSR.
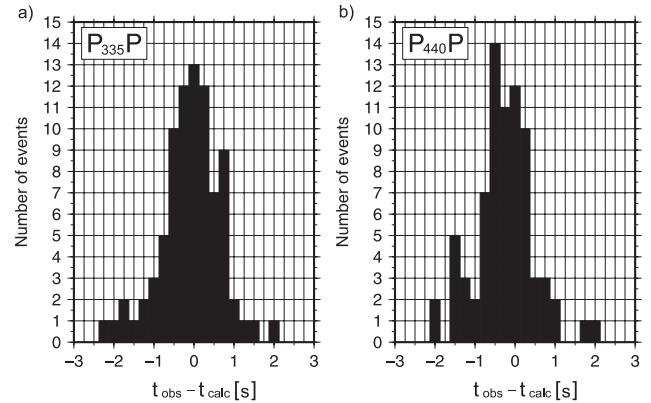
Figure 12. Histograms of the traveltime residuals between the reflected phases $P_{335}P$ (left column), the $P_{440}P$ ones (right column) and the calculated traveltimes for the MP1-SUW model.

Based on the analysis of both the refracted and reflected arrivals, we estimated uncertainty of the velocities in the MP1-SUW model for each layer as $\pm 0.025 \, \text{km s}^{-1}$. The uncertainty for the depth of each discontinuity is $\pm 10 \, \text{km}$.

6 Discussion

The MP1-SUW model is intended to characterize upper mantle structure below the western rim of the EEC. Both 1-D and 2-D models provide a consistent image. The Lehmann 220 km phase, defining the bottom of the low-velocity zone (Lehmann, 1961), is seen as first arrivals for the distance range of 1500–2150 km. A very prominent feature of the MP1-SUW model is the existence of the 300 km discontinuity at the depth of 335 km, which is observed at the 1500–2800 km offset range. The origin of the 300 km discontinuity is generally related to the existence of a subduction zone (Revenaugh and Jordan, 1991), where increased amount of free silica is delivered to the upper mantle by subducted oceanic and continental material. Both coesite–stishovite phase transformation and the thermal anomaly caused by a subducting slab can explain the velocity jump at this discontinuity (Liu et al., 1999). With relation to the mechanical mixture model of Xu et al. (2008), the jump in P wave velocity at approximately 335 km depth would require enrichment in the basaltic component. In this region, the nature of this boundary can be tentatively explained as the traces of the ancient subduction regime related to the closure of the Iapetus and Rheic oceans and the Tornquist Sea (e.g. Torsvik et al., 1996, Torsvik and Rehnström, 2003). This discontinuity, due to its regional scale, is recorded better for the JMR and CR groups of events, although we observe it also for the WMSR and GTR groups. An independent support for the existence of such a discontinuity was recently provided by Knapmeyer-Endrun et al. (2013), who studied the P wave receiver function based on the data from

the PASSEQ experiment. There is a clear peak observed in the receiver function section clustered around TTZ at ca. 30 s relative time (see Fig. 7 in Knapmeyer-Endrun et al., 2013), which is roughly equivalent to ca. 300 km depth. However, authors do not comment whether this signal is related to primary or multiple energy.

We modelled 410 km discontinuity at the depth of 440 km. It is observed as first arrivals in the 2150–3100 km offset range. The deeper location of this discontinuity compared to the reference global model (e.g. AK135) relates to the observation of the LVZ atop it. We find reports of such a zone in regional-scale investigations (Thybo et al., 1997). It was also postulated as the global phenomenon (Bercovici and Karato, 2003). In this case it can also be explained as an ancient oceanic structure subducted during the closure of the Tornquist Sea (Torsvik and Rehnström, 2003). We interpret the low-velocity zone above 410 km discontinuity as a result of the dehydration of the subducted plate that brought some residual water in the transition zone. This feature was found and documented also in the western part of the United States (Song et al., 2004), where authors interpreted it as a compositional anomaly. It could be caused by a dense partially melted layer linked to prior subduction of the Farallon Plate and back-arc extension.

Comparing MP1-SUW model with regional tomographic models based on *P* wave traveltimes like the one of Koulakov et al. (2009), we observe similar pattern of the velocity anomalies in the regions analysed in this paper (Fig. 1b), both in horizontal and vertical slices. However the comparison is not straightforward as the tomographic models are inherently smooth and continuous whereas our model contain discontinuities modelled using reflected waves.

7 Conclusions

We derived a new *P* wave velocity model of the upper mantle structure characterizing the western rim of the East European Craton (model MP1-SUW). Analysing seismic record sections from events recorded at the SUW station, we calculated a one-dimensional *P* wave velocity model for the azimuthally differentiated regions: the Western Mediterranean Sea region, the Greece and Turkey region and the Caucasus region. The two-dimensional model for the JMR region was justified by the fact that waves propagating from that source region travel through the oceanic and continental structures.

The MP1-SUW model documents the bottom of the asthenospheric low-velocity zone at the depth of 220 km, 335 km discontinuity and the zone with the reduction of *P* wave velocity atop 410 km discontinuity which is depressed to 440 km depth. The nature of both the 335 and 440 km discontinuities are explained by tracing the ancient subduction regime related to the closure of the Iapetus and Rheic oceans and the Tornquist Sea (Torsvik and Rehnström, 2003). The 335 km discontinuity is a robust feature of the MP1-SUW

model, however we are aware that this feature is not ubiquitous, but linked to the marginal zone of the EEC.

The work presented here shows that even a single station can be a rich source of information when a careful phase identification and modelling are implemented. We hope that the seismological community can benefit from the use of the MP1-SUW model in other regional studies, for example, in receiver function calculation or traveltime tomography.

Edited by: J. Plomerova

References

Abramovitz, T., Thybo, H., and MONA LISA Working Group: Seismic structure across the Caledonian deformation front along MONA LISA profile 1 in the southeastern North Sea, Tectonophys, 288, 153–176, 1998.

Abramovitz, T., Landes, M., Thybo, H., Jacob, A. W. B., and Prodehl, C.: Crustal velocity structure across the Tornquist and Iapetus Suture Zones – a comparison based on MONA LISA and VARNET data, Tectonophys, 314, 69–82, 1999.

Abramovitz, T., Thybo, H., and Perchuc, E.: Tomographic inversion of seismic *P* and *S* wave velocities from the Baltic Shield based on FENNOLORA data, Tectonophys, 358, 151–174, 2002.

BABEL Working Group: Evidence for early Proterozoic plate tectonics from seismic reflection profiles in the Baltic Shield, Nature, 348, 34–38, 1991.

BABEL Working Group: Deep seismic reflection/refraction interpretation of crustal structure along BABEL profiles A and B in the southern Baltic Sea, Geophys. J. Int., 112, 325–343, 1993.

Bastow, I. D.: Relative arrival-time upper-mantle tomography and the elusive background mean, Geophys. J. Int., 190, 1271–1278, 2012.

Bercovici, D. and Karato, S.: Whole-mantle convection and the transition-zone water filter, Nature, 425, 39–44, 2003.

Bock, G., Perchuc, E., Hanka, W., Wiejacz, P., Kind, R., Suchcicki, J., and Wylengalla, K.: Seismic anisotropy beneath the Suwalki station: one year of the activity of the station, Acta Geophys. Pol., 45, 1–12, 1997.

Bogdanova, S. V., Gorbatschev, R., and Stephenson, R. A.: EURO-BRIDGE: paleoproterozoic accretion of Fennoscandia and Sarmatia, Tectonophys, 339, vii-x, 2001.

Bogdanova, S. V., Gorbatschev, R., and Garetsky, R. G.: The East European craton, in: Encyclopedia of Geology, edited by: Selley, R. C., Cocks, L. R., and Plimer, I. R., Elsevier, 2, 34–49, 2005.

Cammarano, F. and Romanowicz, B.: Radial profiles of seismic attenuation in the upper mantle based on physical models, Geophys. J. Int., 175, 116–134, 2008.

Chu, R., Schmandt, B. and Helmberger D. V.: Upper mantle P velocity structure beneath the Midwestern United States derived from triplicated waveforms, Geochem. Geophys. Geosyst., 13, 1–21, 2012.

Cocks, L. R. M. and Torsvik, T. H.: European geography in a global context from the Vendian to the end of the Palaeozoic, in: European Lithosphere Dynamics, edited by: Gee, D. G. and Stephenson, R. A., Geological Society, London, Memoirs, 32, 83–95, 2006.

Dziewoński, A. and Anderson, D.: Preliminary reference Earth model, Phys. Earth Planet. In., 25, 297–356, 1981.

EUGENO-S Working Group: Crustal structure and tectonic evolution of the transition between the Baltic Shield and the North German Caledonides (the EUGENO-S Project), Tectonophys, 150, 253–348, 1988.

EUROBRIDGE Seismic Working Group: Seismic velocity structure across the Fennoscandia-Sarmatia suture of the East European craton beneath the EUROBRIDGE profile through Lithuania and Belarus, Tectonophys, 314, 193–217, 1999.

Fuchs, K. and Müller, G.: Computation of synthetic seismograms with the reflectivity method and comparison with observations, Geophys. J. Roy. Astr. S., 23, 417–433, 1971.

Gee, D. G.: Tectonic model for central part of scandinavian caledonides, Am. J. of Sci., A275, 468–515, 1975.

Gorman, A. R.: Ray-theoretical seismic traveltime inversion – modifications for a two-dimensional radially parametrized Earth, Geophys. J. Int., 151, 511–516, 2002.

Grad, M., Keller, G. R., Thybo, H., Guterch, A., and POLONAISE Working Group: Lower lithospheric structure beneath the Trans-European Suture Zone from POLONAISE'97 seismic profiles, Tectonophys, 360, 153–168, 2002.

Grad, M., Tiira, T., and ESC Working Group: The Moho depth map of the European Plate, Geophys. J. Int., 176, 279–292, 2009.

Gregersen, S., Voss, P., Nielsen, L. V., Achauer, U., Busche, H., Rabbel, W., and Shomali, Z. H.: Uniqueness of modeling results from teleseismic P wave tomography in Project Tor, Tectonophys, 481, 99–107, 2010.

Guggisberg, B. and Berthelsen, A.: A two-dimensional velocity model for the lithosphere beneath the Baltic Scield and its possible tectonic significance, Terra Cognita, 7, 631–638, 1987.

Guterch, A., Grad, M., Materzok, R., Perchuc, E., and Toporkiewicz, S.: Results of seismic crustal studies in Poland, Publ. Inst. Geophys. Pol. Acad. Sci., 17, 84–89, 1986.

Guterch, A., Grad, M., Materzok, R., and Perchuc, E.: Deep structure of the Earth's crust in the contact zone of the Paleozoic and Precambrian Platforms in Poland (Tornquist-Teisseyre zone), Tectonophys, 128, 251–279, 1996.

Guterch, A., Grad, M., Thybo, H., Keller, G. R., and POLONAISE Working Group: POLONAISE'97 – international seismic experiment between Precambrian and Variscan Europe in Poland, Tectonophys, 314, 101–121, 1999.

Guterch, A., Grad, M., and Keller, G. R.: Seismologists celebrate the new Millennium with an experiment in Central Europe, EOS Trans. AGU, 82, 529, 534–535, 2001.

Guterch, A., Wybraniec, S., Grad, M., Chadwick, R. A., Krawczyk, C. M., Ziegler, P. A., Thybo, H., and Vos, W. D.: Crustal structure and structural framework, in: Petroleum Geological Atlas of the Southern Permian Basin Area, edited by: Doornenbal, J. C. and Stevenson, A. G., EAGE Publications B. V., 11–23, 2010.

Hoffman, P. F.: United Plates of America, the birth of a craton: early proterozoic assembly and growth of Laurentia, Annu. Rev. Earth Pl. Sc., 16, 543–603, 1988.

ISC Bulletin, available at: http://www.isc.ac.uk/iscbulletin (last access: May 2013), 2013.

Kamiński, W. and Müller, G.: Program LAUFZEIT, University of Karlsruhe, 1979.

Kennett, B. L. N. and Engdahl, E. R.: Travel times for global earthquake location and phase identification, Geophys. J. Int., 105, 429–465, 1991.

Kennett, B. L. N., Engdahl, E. R., and Buland, R.: Constraints on seismic velocities in the earth from travel times, Geophys. J. Int, 122, 108–124, 1995.

Knapmeyer-Endrun, B., Krüger, F., Legendre, C., Geissler, W., and PASSEQ Working Group: Tracing the influence of the Trans-European Suture Zone into the mantle transition zone, Earth Planet. Sc. Lett., Elsevier, 363, 73–87, 2013.

Koulakov, I., Kaban, M. K., Tesauro M., and Cloetingh S.: P- and S-velocity anomalies in the upper mantle beneath Europe from tomographic inversion of ISC data, Geophys. J. Int., 179, 345–366, 2009.

Liu, J., Zhang, J., Flesch, L., Li, B., Weidner, D., and Liebermann, R.: Thermal equation of state of stishovite, Phys. Earth Planet. In., 112, 257–266, 1999.

Lehmann, I.: S and the Structure of the Upper Mantle, Geophys. J. Roy. Astr. S., 4, 124–138, 1961.

Levander, A.: USArray design implications for wavefield imaging in the lithosphere and upper mantle, The Leading Edge, 22, 250–255, 2003.

Müller, G.: The reflectivity method: a tutorial, J. Geophys., 58, 153–174, 1985.

Nita, B., Dobrzhinetskaya, L., Maguire, P., and Perchuc, E.: Age-differentiated subduction regime: An explanation of regional scale upper mantle differences beneath the Alps and the Variscides of Central Europe, Phys. Earth Planet. In., 206–207, 1–1, 2012.

Perchuc, E. and Thybo, H.: A new model of upper mantle P waves velocity below the Baltic Shield, Indication of partial melt in the 95 to 160 km depth range, Tectonophys, 253, 227–245, 1996.

Perchuc, E., Malinowski, M., and Nita, B.: Seismic and petrological properties of the upper mantle between 300 and 400 km depth, AGU Fall Meeting, S14C-01, 2008.

Plomerová, J., Babuška, V., Vecsey, L., and Kouba, D.: Seismic anisotropy of the lithosphere around the Trans-European Suture Zone (TESZ) based on teleseismic body-wave data of the TOR experiment, Tectonophys, 360, 89–114, 2002.

Revenaugh, J. and Jordan, T.: Mantle layering from ScS reverberations: the upper mantle, J. Geophys. Res., 96, 19781–19810, 1991.

Shapiro, N. M. and Ritzwoller, M. H.: Monte-Carlo inversion for a global shear velocity model of the crust and upper mantle, Geophys. J. Int., 151, 1–18, 2002.

Song, T. A., Helmberger, D. V., and Grand, S. P.: Low-velocity zone atop the 410 km seismic discontinuity, Nature, 427, 530–533, 2004.

Somali, Z. H., Roberts, R. G., Pedersen, L. B., and the TOR Working Group: Lithospheric structure of the Tornquist Zone resolved by nonlinear P and S teleseismic tomography along the TOR array, Tectonophys, 416, 133–149, 2006.

Świeczak, M., Grad, M., and TOR and SVEKALAPKO Working Groups: upper mantle seismic discontinuities: topography variations beneath Eastern Europe, Acta Geophys. Pol., 52, 251–270, 2004.

Thybo, H. and Perchuc, E.: The seismic 8° discontinuity and partial melting in continental mantle, Science, 275, 1626–1629, 1997.

Thybo, H., Perchuc, E., and Pavlenkova, N.: Two Reflectors in the 400 km Depth Range Revealed from Peaceful Nuclear Explosion Seismic Sections, Upper Mantle Heterogeneities from Active and Passive Seismology, edited by: Fuchs, K., NATO ASI Series, 97–104, 1997.

Torsvik, T. H., Smethurst, M. A., Meert, J. G., Van der Voo, R., McKerrow, W. S., Brasier, M. D., Sturt, B. A., and Walderhaug. H. J.: Continental break-up and collision in the Neoproterozoic and Palaeozoic: a tale of Baltica and Laurentia, Earth-Sci. Rev., 40, 229–258, 1996.

Torsvik, T. H. and Rehnström, E. F.: The Tornquist Sea and Baltica-Avalonia docking, Tectonophys, 362, 67–82, 2003.

Wessel, P. and Smith, W. H. F.: New version of Generic Mapping Tools released, EOS, 76, 453, 1995.

Wilde-Piórko, M.: Crustal structure from seismic receiver function, Przegląd Geofizyczny, 1–2, 31–45, 2005.

Wilde-Piórko, M., Geissler, W., Plomerová, J., Grad, M., Babuška, V., Brückl, E., Cyziene, J., Czuba, W., England, R., Gaczyński, E., Gazdova, R., Gregersen, S., Guterch, A., Hanka, W., Hegedűs, E., Heuer, B., Jedlička, P., Lazauskiene, J., Keller, G., Kind, R., Klinge, K., Kolinsky, P., Komminaho, K., Kozlovskaya, E., Krüger, F., Larsen, T., Majdański, M., Malek, J., Motuza, G., Novotný, O., Pietrasiak, R., Plenefisch, T., Růžek, B., Sliaupa, S., Środa, P., Świeczak, M., Tiira, T., Voss, P., and Wiejacz, P.: PASSEQ 2006–2008: Passive seismic experiment in Trans-European Suture Zone, Studia Geophysica et Geodetica, 52, 439–448, 2008.

Xu, W., Lithgow-Bertelloni, C., Stixrude, L., and Ritsema, J.: The effect of bulk composition and temperature on mantle seismic structure, Earth Planet. Sci. Lett., 275, 70–79, 2008.

Zelt, C.: ZPLOT – an iterative plotting and picking program for seismic data, Bullard Lab. Univ. of Cambridge, Cambridge UK, 1994.

Ziegler, P. A. and Dèzes, P.: Crustal configuration of Western and Central Europe, in: European Lithosphere Dynamics, edited by: Gee, D. G. and Stephenson, R. A., Geol. Soc., London, Memoirs 32, 43–56, 2006.

Znosko, J.: Polish Caledonides and their relation to other European Caledonides, Ann. Soc. Geol. Pol., 56, 33–52, 1986.